energies

MDPI

Article

Coupling Influence on the dq Impedance Stability Analysis for the Three-Phase Grid-Connected Inverter

Chuanyue Li [1], Taoufik Qoria [1], Frederic Colas [1], Jun Liang [2], Wenlong Ming [2], Francois Gruson [1] and Xavier Guillaud [1,*]

[1] Laboratory of Electricl Engineering and Power Electronics (L2EP), 59046 Lille, France; Chuanyue.Li@outlook.com (C.L.); taoufik.qoria@ensam.eu (T.Q.); Frederic.COLAS@ENSAM.eu (F.C.); francois.gruson@ensam.eu (F.G.)

[2] School of Engineering, Cardiff University, Cardiff CF24 3AA, UK; Liangj1@Cardiff.ac.uk (J.L.); MingW@cardiff.ac.uk (W.M.)

* Correspondence: xavier.guillaud@centralelille.fr

Received: 1 August 2019; Accepted: 23 September 2019; Published: 26 September 2019

Abstract: The dq impedance stability analysis for a grid-connected current-control inverter is based on the impedance ratio matrix. However, the coupled matrix brings difficulties in deriving its eigenvalues for the analysis based on the general Nyquist criterion. If the couplings are ignored for simplification, unacceptable errors will be present in the analysis. In this paper, the influence of the couplings on the dq impedance stability analysis is studied. To take the couplings into account simply, the determinant-based impedance stability analysis is used. The mechanism between the determinant of the impedance-ratio matrix and the inverter stability is unveiled. Compared to the eigenvalues-based analysis, only one determinant rather than two eigenvalue s-function is required for the stability analysis. One Nyquist plot or pole map can be applied to the determinant to check the right-half-plane poles. The accuracy of the determinant-based stability analysis is also checked by comparing with the state-space stability analysis method. For the stability analysis, the coupling influence on the current control, the phase-locked loop, and the grid impedance are studied. The errors can be 10% in the stability analysis if the couplings are ignored.

Keywords: impedance stability analysis; VSC; small-signal modelling

1. Introduction

The integration of renewable energy sources is normally assisted by power electronic converters due to its ability for asynchronous connection and fully-AC voltage control. The high demand for renewable energies requires more and more inverters to be connected to the grid. The interaction between the grid-connected inverter and the grid may cause instabilities [1]. The stability analysis for the grid-connected inverter is essential to ensure secure power transportation to the grid.

Two stability analysis methods can be applied according to the small-signal linearization technology. The state-space stability analysis [2] is a mature and commonly-used method. However, a high order and a complex state matrix have to be built. Impedance stability analysis is achieved via the impedance ratio, which is determined via the equivalent impedance of the inverter and the grid impedance. The impedance ratio can also be drawn as the Bode plot for the frequency analysis. Both Norton-based [3] and Thevenin-based [4] equivalent impedances of the inverter can be derived in the impedance stability analysis.

For a three-phase inverter controlled via the dq frame, the impedance ratio is normally derived in the dq frame, which is a 2×2 matrix. Both eigenvalues of the impedance-ratio matrix are required for the stability analysis via the generalized Nyquist criterion (GNC) [5]. The criterion is commonly used

in the grid-connected inverter system to identify the negative impact on the stability, such as increasing the cut-off frequency of the phase-locked loop (PLL) [6] and current control loop [7], increasing power injection from the inverter and grid impedance [8]. For a grid-connected current control inverter, only the q-axis is used for the PLL to synchronize the dq frame. Therefore, its impedance-ratio matrix is a coupled asymmetrical matrix, whose eigenvalues are difficult to derive. Couplings are normally ignored to simplify the eigenvalue derivation during the impedance stability analysis [8,9]. To achieving an accurate impedance stability analysis based on GNC, the impedance-ratio matrix is transferred into the stationary frame in order to decouple the matrix [10]. However, it is found that couplings still exist because the impedance-ratio matrix is asymmetrical [11].

The determinant, rather than both eigenvalues of the impedance-ratio matrix, which is derived simply for including couplings, was used for the three-phase rectifier's stability analysis [12,13] in the 1990s. Recently, the impedance stability analysis based on the determinant was applied for the inverter system [14,15]. Only the determinant, rather than two eigenvalues, is figured as one pole map or one Nyquist plot for the stability analysis, which simplifies the analysis process. Another method for including couplings is to convert the multi-input and multi-output dq impedance into its sequence domain single-input and single-output equivalents [16]. Then, the Nyquist criterion, rather than the generalized Nyquist criterion, can be applied.

In this paper, the coupling influence on the dq impedance stability analysis is studied. The question about whether ignoring couplings causes unacceptable analysis errors will be answered. Analysis errors are defined and quantified to assist the study of the coupling influence. The dq impedance stability analysis based on the determinant rather than eigenvalues is used to include the couplings easily and present the accurate analysis results. The mechanism by which the stability of the inverter system is determined only by the determinant of the impedance-ratio matrix will be unveiled. The dq impedance stability analysis results will be validated in the time-domain simulation. The state-space stability analysis will be used as the benchmark to validate the accuracy of the determinant-based impedance stability analysis.

This paper is organized as follows: In Section 2, the dq impedance stability analysis is introduced. The equivalent dq impedance of the inverter is derived in Section 3. The simulation verification and the coupling influence are shown in Section 4.

2. dq Impedance Stability Analysis

Grid-connected inverters are normally controlled in the dq frame as a current source. Therefore, its small-signal model is built according to the Norton law [3], as shown in Figure 1. A list of variables, which are shown in Figure 1, is explained below:

- $\widetilde{\mathbf{i}}_s$: reference deviation of the control system
- $\widetilde{\mathbf{v}}_o$: output voltage deviation
- $\widetilde{\mathbf{i}}_g$: feeding current deviation from the inverter
- $\mathbf{Z}_g$: grid impedance
- $\widetilde{\mathbf{v}}_g$: grid voltage deviation
- $\mathbf{Y}_o$: equivalent inverter admittance
- the bold variables stand for its d-q matrix such as $\widetilde{\mathbf{i}}_g = \begin{bmatrix} \widetilde{i}_{gd} \\ \widetilde{i}_{gq} \end{bmatrix}$.

The frequently-used notations are summarized below:

- d,q: d-axis and q-axis parameters
- dd, dq, qd, qq: the postion of each element in the matrix
- rt: ratio matrix
- u,l: upper and lower parameters

From the inverter side, the relation between $\widetilde{\mathbf{v}}_o$ and $\widetilde{\mathbf{i}}_g$ is derived as:

$$\widetilde{\mathbf{i}}_g = \widetilde{\mathbf{i}}_s + \mathbf{Y}_o \widetilde{\mathbf{v}}_o \tag{1}$$

From the grid side, the relation between $\widetilde{\mathbf{i}}_g$ and $\widetilde{\mathbf{v}}_g$ is derived as:

$$\widetilde{\mathbf{v}}_o - \widetilde{\mathbf{v}}_g = \mathbf{Z}_g \widetilde{\mathbf{i}}_g \tag{2}$$

Substituting $\widetilde{\mathbf{i}}_g$ in (2) with (1) yields:

$$\widetilde{\mathbf{v}}_o = \mathbf{Z}_g \widetilde{\mathbf{i}}_s + \mathbf{Z}_g \mathbf{Y}_o \widetilde{\mathbf{v}}_o + \widetilde{\mathbf{v}}_g \tag{3}$$

Rearranging (3) for $\widetilde{\mathbf{v}}_o$ yields:

$$\widetilde{\mathbf{v}}_0 = (\mathbf{I} - \mathbf{Z}_g \mathbf{Y}_o)^{-1} (\widetilde{\mathbf{v}}_g + \mathbf{Z}_g \widetilde{\mathbf{i}}_s) \tag{4}$$

where the impedance-ratio matrix is $(\mathbf{I} - \mathbf{Z}_g \mathbf{Y}_o)^{-1}$.

It is reported [3] that the system stability is determined by the impedance-ratio matrix $(\mathbf{I} - \mathbf{Z}_g \mathbf{Y}_o)^{-1}$ based on (4).

2.1. *dq Impedance Stability Analysis via Eigenvalues*

Based on the generalized Nyquist criterion, both eigenvalues of the impedance-ratio matrix need to be drawn as Nyquist plots for the stability analysis [8].

Each element of the impedance-ratio matrix is presented below:

$$(\mathbf{I} - \mathbf{Z}_g \mathbf{Y}_o)^{-1} = \begin{bmatrix} Y_{dd}^{rt}(s) & Y_{dq}^{rt}(s) \\ Y_{qd}^{rt}(s) & Y_{qq}^{rt}(s) \end{bmatrix} \tag{5}$$

where notation dd, dq, qd, and qqmeans the postion of each element in the matrix, rt means the ratio matrix, and $Y_{dq}^{rt}(s)$, $Y_{qd}^{rt}(s)$ are couplings.

The eigenvalues $\lambda_1(s)\&\lambda_2(s)$ of the matrix are calculated as:

$$\begin{vmatrix} \lambda_1(s) - Y_{dd}^{rt}(s) & Y_{dq}^{rt}(s) \\ Y_{qd}^{rt}(s) & \lambda_2(s) - Y_{qq}^{rt}(ss) \end{vmatrix} = 0 \tag{6}$$

The transfer functions of the eigenvalues are found by rearranging the equation above:

$$\lambda_1(s), \lambda_2(s) = \frac{Y_{dd}^{rt}(s) + Y_{qq}^{rt}(s)}{2} \pm \frac{\sqrt{(Y_{dd}^{rt}(s) - Y_{qq}^{rt}(s))^2 + 4Y_{dq}^{rt}(s)Y_{qd}^{rt}(s)}}{2} \tag{7}$$

It is difficult to do the square root of $\dfrac{\sqrt{(Y_{dd}^{rt}(s) - Y_{qq}^{rt}(s))^2 + 4Y_{dq}^{rt}(s)Y_{qd}^{rt}(s)}}{2}$ in (7), as each element of the impedance-ratio matrix is a complicated transfer function in the s domain. If the couplings $Y_{dq}^{rt}(s)$, $Y_{qd}^{rt}(s)$ are ignored, eigenvalues are therefore simplified and calculated below based on (7):

$$\lambda_1(s) = Y_{dd}^{rt}(s) \quad \lambda_2(s) = Y_{qq}^{rt}(s) \tag{8}$$

The ignoration removes the coupling influence on the system stability analysis. The stability analysis will be more accurate if the couplings are considered.

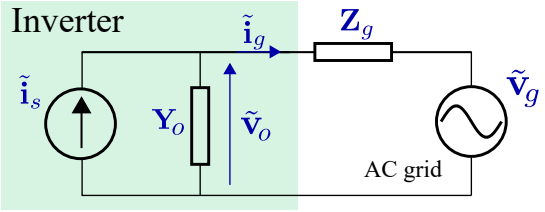

Figure 1. Equivalent small-signal model of a grid-connected inverter with dq frame control.

2.2. *dq Impedance Stability Analysis via the Determinant*

It was found that the determinant of the impedance-ratio matrix is the key factor that determines the system stability. Couplings of the impedance-ratio matrix are contained in the determinant; thus, their influences on the stability are all accounted for. The Nyquist plot or the pole map as the stability analysis tool can be drawn via the determinant to check the right-plane poles. The mechanism of the determinant as the key factor for the stability analysis is shown below.

The impedance-ratio matrix can be reconstructed as two parts: an adjacent matrix and a determinant as shown below:

$$(\mathbf{I} - \mathbf{Z}_g\mathbf{Y}_o)^{-1} = \text{adj}(\mathbf{I} - \mathbf{Z}_g\mathbf{Y}_o)\det((\mathbf{I} - \mathbf{Z}_g\mathbf{Y}_o)^{-1}) \tag{9}$$

The adjacent matrix is calculated based on (5):

$$\text{adj}(\mathbf{I} - \mathbf{Z}_g\mathbf{Y}_o) = \begin{bmatrix} Y^{rt}_{qq}(s) & -Y^{rt}_{dq}(s) \\ -Y^{rt}_{qd}(s) & Y^{rt}_{dd}(s) \end{bmatrix} \tag{10}$$

Each element of $\mathbf{Y}_o$ and $\mathbf{Z}_g$ is rewritten as the form such as $\frac{Y^o_{ddu}(s)}{Y^o_{ddl}(s)}$, where the numerator $Y^o_{ddu}(s)$ stands for all its zeros and the denominator $Y^o_{ddl}(s)$ stands for all its poles as shown below:

$$Y^o_{ddu}(s) = (s + z_1)\cdots(s + z_n) \tag{11}$$

$$Y^o_{ddl}(s) = (s + p_1)\cdots(s + p_m) \tag{12}$$

where n and m are the number of zeros and poles, respectively.

The equivalent admittance $\mathbf{Y}_o$ of the inverter and the impedance $\mathbf{Z}_g$ of the grid can be presented as below:

$$\mathbf{Y}_o = \begin{bmatrix} \frac{Y^o_{ddu}(s)}{Y^o_{ddl}(s)} & \frac{Y^o_{dqu}(s)}{Y^o_{dql}(s)} \\ \frac{Y^o_{qdu}(s)}{Y^o_{qdl}(s)} & \frac{Y^o_{qqu}(s)}{Y^o_{qql}(s)} \end{bmatrix} \tag{13}$$

$$\mathbf{Z}_g = \begin{bmatrix} \frac{Z^g_{ddu}(s)}{Z^g_{ddl}(s)} & \frac{Z^g_{dqu}(s)}{Z^g_{dql}(s)} \\ \frac{Z^g_{qdu}(s)}{Z^g_{qdl}(s)} & \frac{Z^g_{qqu}(s)}{Z^g_{qql}(s)} \end{bmatrix} \tag{14}$$

One element of adj$(\mathbf{I} - \mathbf{Z}_g\mathbf{Y}_o)$ such as $Y^{rt}_{dd}(s)$ will be calculated based on (10), (13), and (14):

$$Y^{rt}_{dd}(s) = \frac{Y^{rt}_{ddu}(s)}{Y^{rt}_{ddl}(s)} = 1 - \left(\frac{Z^{g}_{ddu}(s)}{Z^{g}_{ddl}(s)} \times \frac{Y^{o}_{ddu}(s)}{Y^{o}_{ddl}(s)} + \frac{Z^{g}_{dqu}(s)}{Z^{g}_{dql}(s)} \times \frac{Y^{o}_{qdu}(s)}{Y^{o}_{qdl}(s)}\right) \tag{15}$$

All poles of Y^{rt}_{ddl} can be derived from (15):

$$Y^{rt}_{ddl}(s) = Y^{o}_{ddl}(s)Z^{g}_{ddl}(s)Y^{o}_{dql}(s)Z^{g}_{qdl}(s) \tag{16}$$

The equivalent admittance $\mathbf{Y}_o$ of the inverter has no right-plane poles ([3]), neither the grid impedance $\mathbf{Z}_g$. Therefore, no right-plane poles exist in $Y^{o}_{ddl}(s)$, $Z^{g}_{ddl}(s)$, $Y^{o}_{dql}(s)$, and $Z^{g}_{qdl}(s)$. It can be identified via (16) that $Y^{rt}_{dd}(s)$ has no right-plane poles. Following the same way, the other elements of adj$(\mathbf{I} - \mathbf{Y}_o\mathbf{Z}_g)$ have no right-plane poles.

It can be concluded finally via the identification above and (9) that the system stability is determined only by the determinant $\det((\mathbf{I} - \mathbf{Y}_o\mathbf{Z}_g)^{-1})$ of the impedance-ratio matrix. For the stability analysis, one Nyquist plot or one pole map can be used based on the determinant for the stability analysis by checking the right-plane poles.

3. Small Signal Impedance of a Current-Controlled Inverter

Before validating the accuracy of the determinant-based stability analysis, $\mathbf{Y}_o$ of the grid-connected inverter will be derived in this section. The grid-connected inverter is usually controlled in the dq frame as a current source, and the frame is synchronized via a PLL, as shown in Figure 2. The abc-dq transformation in terms of the PLL is linearized first, and the impedance derivation is followed. The variables are shown in Figure 2 and are listed and explained below to help define the equations.

- T_{del}: time delay from the control and pulse width modulation (PWM) dead time.
- θ: synchronized phase from PLL.
- $\mathbf{V}_c = \begin{bmatrix} V_{cd} \\ V_{cq}. \end{bmatrix}$: inverter voltage
- $\mathbf{i}_c = \begin{bmatrix} i_{cd} \\ i_{cq}. \end{bmatrix}$: inverter current
- $\mathbf{v}_o = \begin{bmatrix} v_{od} \\ v_{oq}. \end{bmatrix}$: output voltage
- $\mathbf{V}^s_c = \begin{bmatrix} V^s_{cd} \\ V^s_{cq}. \end{bmatrix}$: inverter voltage after abc-dq transform
- $\mathbf{i}^s_c = \begin{bmatrix} i^s_{cd} \\ i^s_{cq}. \end{bmatrix}$: inverter current after abc-dq transform
- $\mathbf{v}^s_o = \begin{bmatrix} v^s_{od} \\ v^s_{oq}. \end{bmatrix}$: output voltage after abc-dq transform,
- $k^p_i + \frac{k^i_i}{s}$: PI controller for the current loop.
- $k^p_{PLL} + \frac{k^i_{PLL}}{s}$: PI controller for PLL.
- $\mathbf{Z}_f = \begin{bmatrix} L_f s + R_f & -\omega L_f \\ \omega L_f & L_f s + R_f \end{bmatrix}$: impedance of LC filter.
- $\mathbf{Y}_c = \begin{bmatrix} C_f s & -\omega C_f \\ \omega C_f & C_f s. \end{bmatrix}$: admittance of LC filter.

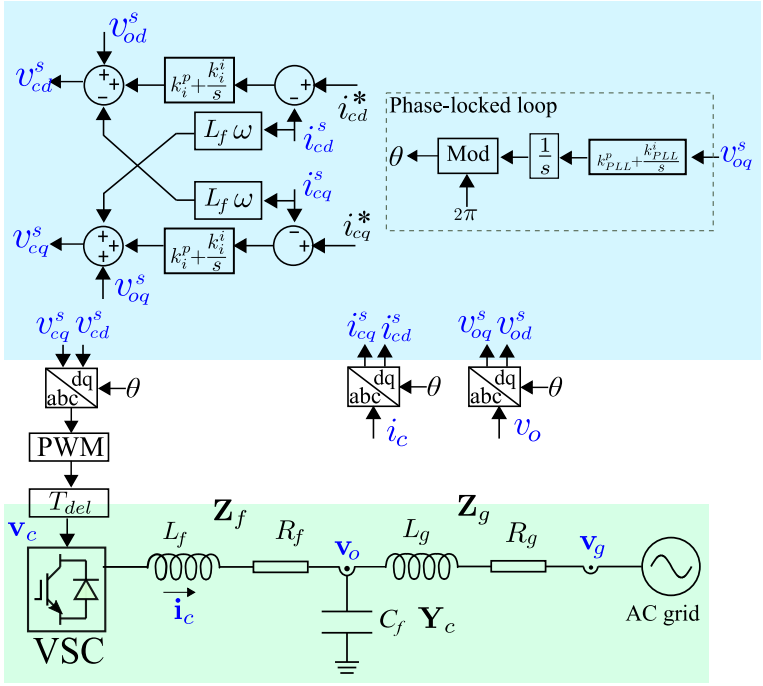

Figure 2. The grid-connected inverter with current control.

3.1. Linearization of the abc-dq Transformation

It is convenient to derive the impedance of the inverter in the dq frame due to the applied dq control. The three-phase abc system is therefore presented as the dq form in the derivation. Theses dq-presented abc parameters ($\mathbf{v}_o$ $\mathbf{i}_c$ $\mathbf{v}_c$) are equal to their dq parameters ($\mathbf{v}_o^s$ $\mathbf{i}_c^s$ $\mathbf{v}_c^s$) after the abc-dq transformation at steady state, but are different when a synchronized phase error $\tilde{\theta}$ is applied at the transformation.

Their relations that take $\mathbf{v}_o^s$ as an example are summarized below via the small-signal modelling:

$$\begin{bmatrix} V_{od}^s + \tilde{v}_{od}^s \\ V_{oq}^s + \tilde{v}_{oq}^s \end{bmatrix} = \begin{bmatrix} \cos\tilde{\theta} & \sin\tilde{\theta} \\ -\sin\tilde{\theta} & \cos\tilde{\theta} \end{bmatrix} \begin{bmatrix} V_{od} + \tilde{v}_{od} \\ V_{oq} + \tilde{v}_{oq} \end{bmatrix} \tag{17}$$

where $\mathbf{V}_o$ and $\mathbf{V}_o^s$ are the corresponding steady state values.

Equation (17) can be linearized as below due to the small value of $\tilde{\theta}$,

$$\begin{bmatrix} V_{od}^s + \tilde{v}_{od}^s \\ V_{oq}^s + \tilde{v}_{oq}^s \end{bmatrix} \approx \begin{bmatrix} 1 & \tilde{\theta} \\ -\tilde{\theta} & 1 \end{bmatrix} \begin{bmatrix} V_{od}^s + \tilde{v}_{od} \\ V_{oq}^s + \tilde{v}_{oq} \end{bmatrix} \tag{18}$$

$\mathbf{V}_o$ and $\mathbf{V}_o^s$ are equal at steady state, and (18) is therefore simplified as:

$$\begin{bmatrix} \tilde{v}_{od}^s \\ \tilde{v}_{oq}^s \end{bmatrix} = \begin{bmatrix} V_{oq}\tilde{\theta} + \tilde{v}_{od} \\ -V_{od}\tilde{\theta} + \tilde{v}_{oq} \end{bmatrix} \tag{19}$$

Following the same way, the relationship between $\tilde{\mathbf{i}}_c^s$ and $\tilde{\mathbf{i}}_c$ is derived:

$$\begin{bmatrix} \tilde{i}_{cd}^s \\ \tilde{i}_{cq}^s \end{bmatrix} = \begin{bmatrix} I_{cq}\tilde{\theta} + \tilde{i}_{cd} \\ -I_{cd}\tilde{\theta} + \tilde{i}_{cq} \end{bmatrix} \tag{20}$$

Considering the dq-abc transformation for the dq-presented inverter voltage $\widetilde{\mathbf{v}}_c$, this yields:

$$\begin{bmatrix} \widetilde{v}_{cd} \\ \widetilde{v}_{cq} \end{bmatrix} = \begin{bmatrix} -V_{cq}\widetilde{\theta} + \widetilde{v}^s_{cd} \\ V_{cd}\widetilde{\theta} + \widetilde{v}^s_{cq} \end{bmatrix} \tag{21}$$

3.2. Small-Signal Model of the Phase-Locked Loop

The synchronized-phase error as the output of the phase-locked loop is generated by its input $\widehat{v}^q_s$. Their relation is summarized as below according to the control diagram Figure 2:

$$\widetilde{\theta} = \widetilde{v}^s_{oq} \times tf_{PLL}(s) \times \frac{1}{s} \tag{22}$$

where $tf_{PLL}(s) = K^p_{PLL} + \dfrac{K^i_{PLL}}{s}$. Notation PLL stands for phase-locked loop; notation p and i are the proportion parameter and the integration parameter of the PI controller, respectively.

Substituting $\widetilde{v}^s_{oq}$ in (22) with (19) yields:

$$\widetilde{\theta} = \underbrace{\frac{tf_{PLL}(s)}{s + V_{od} \times tf_{PLL}(s)}}_{G_{PLL}(s)} \widetilde{v}_{oq} \tag{23}$$

Substituting $\widetilde{\theta}$ in (19)–(21) with (23) yields:

$$\begin{bmatrix} \widetilde{V}^s_{od} \\ \widetilde{V}^s_{oq} \end{bmatrix} = \underbrace{\begin{bmatrix} 1 & V_{oq}G_{PLL}(s) \\ 0 & 1 - V_{od}G_{PLL}(s) \end{bmatrix}}_{\mathbf{G}^{vo}_{PLL}} \begin{bmatrix} \widetilde{V}_{od} \\ \widetilde{V}_{oq} \end{bmatrix} \tag{24}$$

$$\begin{bmatrix} \widetilde{i}^s_{cd} \\ \widetilde{i}^s_{cq} \end{bmatrix} = \underbrace{\begin{bmatrix} 0 & I_{cq}G_{PLL}(s) \\ 0 & -I_{cd}G_{PLL}(s) \end{bmatrix}}_{\mathbf{G}^{ic}_{PLL}} \begin{bmatrix} \widetilde{v}_{od} \\ \widetilde{v}_{oq} \end{bmatrix} + \begin{bmatrix} \widetilde{i}_{cd} \\ \widetilde{i}_{cq} \end{bmatrix} \tag{25}$$

$$\begin{bmatrix} \widetilde{v}_{cd} \\ \widetilde{v}_{cq} \end{bmatrix} = \underbrace{\begin{bmatrix} 0 & -V_{cq}G_{PLL}(s) \\ 0 & V_{cd}G_{PLL}(s) \end{bmatrix}}_{\mathbf{G}^{vc}_{PLL}} \begin{bmatrix} \widetilde{v}_{od} \\ \widetilde{v}_{oq} \end{bmatrix} + \begin{bmatrix} \widetilde{v}^s_{cd} \\ \widetilde{v}^s_{cq} \end{bmatrix} \tag{26}$$

Equations (24)–(26) present the fully-linearized relation between the dq parameters and the dq-presented abc parameters.

3.3. Inverter Admittance Derivation

After the linearization, the current control, LC filter, and grid impedance will be accounted for in the derivation for the final admittance of the inverter. The current control is presented below according to Figure 2:

$$\mathbf{tf}_i(s)(\widetilde{\mathbf{i}}^*_c - \widetilde{\mathbf{i}}^s_c) + \mathbf{G}_{dei}\widetilde{\mathbf{i}}^s_c + \widetilde{\mathbf{v}}^s_o = \widetilde{\mathbf{v}}^s_c \tag{27}$$

where $\mathbf{tf}_i(s) = \begin{bmatrix} K^p_i + \dfrac{K^i_i}{s} & 0 \\ 0 & K^p_i + \dfrac{K^i_i}{s} \end{bmatrix}$, $\mathbf{G}_{dei} = \begin{bmatrix} 0 & -\omega L_f \\ \omega L_f & 0 \end{bmatrix}$.

Substituting $\widetilde{\mathbf{i}}_c^s$, $\widetilde{\mathbf{v}}_o^s$ in (27) with (24) and (25) yields:

$$\mathbf{tf}_i(s)(\widetilde{\mathbf{i}}_c^* - (\mathbf{G}_{PLL}^{i_c}\widetilde{\mathbf{v}}_o + \widetilde{\mathbf{i}}_c)) + \mathbf{G}_{dei}(\mathbf{G}_{PLL}^{i_c}\widetilde{\mathbf{v}}_o + \widetilde{\mathbf{i}}_c) + \mathbf{G}_{PLL}^{v_o}\widetilde{\mathbf{v}}_o = \widetilde{\mathbf{v}}_c^s \tag{28}$$

Substituting $\widetilde{\mathbf{v}}_c^s$ in (26) with (28) and taking the time T_{del} including control delay and the dead time of PWM into account yields:

$$\mathbf{G}_{del}[\mathbf{tf}_i(s)(\widetilde{\mathbf{i}}_c^* - (\mathbf{G}_{PLL}^{i_c}\widetilde{\mathbf{v}}_o + \widetilde{\mathbf{i}}_c)) + \mathbf{G}_{dei}(\mathbf{G}_{PLL}^{i_c}\widetilde{\mathbf{v}}_o + \widetilde{\mathbf{i}}_c) + \mathbf{G}_{PLL}^{v_o}\widetilde{\mathbf{v}}_o + \mathbf{G}_{PLL}^{v_c}\widetilde{\mathbf{v}}_o] = \widetilde{\mathbf{v}}_c \tag{29}$$

where $\mathbf{G}_{del} = \begin{bmatrix} \frac{1-0.5T_{del}s}{1+0.5T_{del}s} & 0 \\ 0 & \frac{1-0.5T_{del}s}{1+0.5T_{del}s} \end{bmatrix}$

$\widetilde{\mathbf{i}}_c$ can be presented as the crossing voltage over $\mathbf{Z}_f$:

$$\mathbf{Z}_f\widetilde{\mathbf{i}}_c = \widetilde{\mathbf{v}}_c - \widetilde{\mathbf{v}}_o \tag{30}$$

Substituting $\widetilde{\mathbf{v}}_c$ in (29) with (30) and rearranging yield:

$$\mathbf{tf}_i(s)\mathbf{G}_{del}\widetilde{\mathbf{i}}_c^* + [\mathbf{G}_{del}(-\mathbf{tf}_i(s)\mathbf{G}_{PLL}^{i_c} + \mathbf{G}_{dei}\mathbf{G}_{PLL}^{i_c} + \mathbf{G}_{PLL}^{v_o} + \mathbf{G}_{PLL}^{v_c}) - \mathbf{I}]\widetilde{\mathbf{v}}_o = [\mathbf{G}_{del}(\mathbf{tf}_i(s) - \mathbf{G}_{dei}) + \mathbf{Z}_f]\widetilde{\mathbf{i}}_c \tag{31}$$

Rewriting (31) yields:

$$\widetilde{\mathbf{i}}_c = \mathbf{G}_{ref}\widetilde{\mathbf{i}}_c^* + \mathbf{Y}_b\widetilde{\mathbf{v}}_o \tag{32}$$

where $\mathbf{G}_{ref} = [\mathbf{G}_{del}(\mathbf{tf}_i(s) - \mathbf{G}_{dei}) + \mathbf{Z}_f]^{-1}\mathbf{tf}_i(s)\mathbf{G}_{del}$, $\mathbf{Y}_b = [\mathbf{G}_{del}(\mathbf{tf}_i(s) - \mathbf{G}_{dei}) + \mathbf{Z}_f]^{-1}[\mathbf{G}_{del}(-\mathbf{tf}_i(s)\mathbf{G}_{PLL}^{i_c} + \mathbf{G}_{dei}\mathbf{G}_{PLL}^{i_c} + \mathbf{G}_{PLL}^{v_o} + \mathbf{G}_{PLL}^{v_c}) - \mathbf{I}]$

Considering the influence of the capacitor of the LC filter yields:

$$\widetilde{\mathbf{i}}_g = \widetilde{\mathbf{i}}_c - \mathbf{Y}_c\widetilde{\mathbf{v}}_o \tag{33}$$

Substituting $\widetilde{\mathbf{i}}_c$ in (32) with (33) yields:

$$\widetilde{\mathbf{i}}_g = \underbrace{(\mathbf{Y}_b - \mathbf{Y}_c)}_{\mathbf{Y}_o}\widetilde{\mathbf{v}}_o + \underbrace{\mathbf{G}_{ref}\widetilde{\mathbf{i}}_c^*}_{\widetilde{\mathbf{i}}_s} \tag{34}$$

It is found based on (1) that $\mathbf{Y}_o$ is $\mathbf{Y}_b - \mathbf{Y}_c$, and $\widetilde{\mathbf{i}}_s$ is $\mathbf{G}_{ref}\widetilde{\mathbf{i}}_c^*$. Therefore, $\mathbf{Y}_o$ has been derived based on the above equations, and the dq impedance stability analysis based on the determinant can be applied.

3.4. Comparison between Determinant-Based Impedance Stability Analysis and State-Space Stability Analysis

It is essential to validate the accuracy of the determinant-based impedance stability analysis. Therefore, the state-space stability analysis, as a benchmark of the stability analysis [2], is used for the validation. The derivation for the state-space stability analysis is shown in the Appendix A. The grid-connected current-controlled inverter system for the stability analysis is shown in Figure 2, and its parameters are shown in Table 1. The inductors and resistors of the AC transformer (L_c, R_t) and the transmission line (SCR) are noted as L_g and R_g in Figure 2.

The pole map is used for the comparison between both stability analyses because it shows the pole position and pole locus in detail and simply. For the determinant-based impedance stability analysis, all the poles of the determinant based on (9) are drawn in the pole map.

The pole locus of both stability analyses are drawn in Figure 3 by changing the cut-off frequency of PLL (ω_{PLL}) from 55 rad/s to 1100 rad/s. As shown in Figure 3, the pole locus and each pole of both

stability analyses are precisely matched. The same stability analysis result based on their pole locus is found, that increasing ω_{PLL} leads the poles towards to the right-half plane and causes the low stability or instability of the inverter system. It is concluded that both stability analyses have the same accuracy.

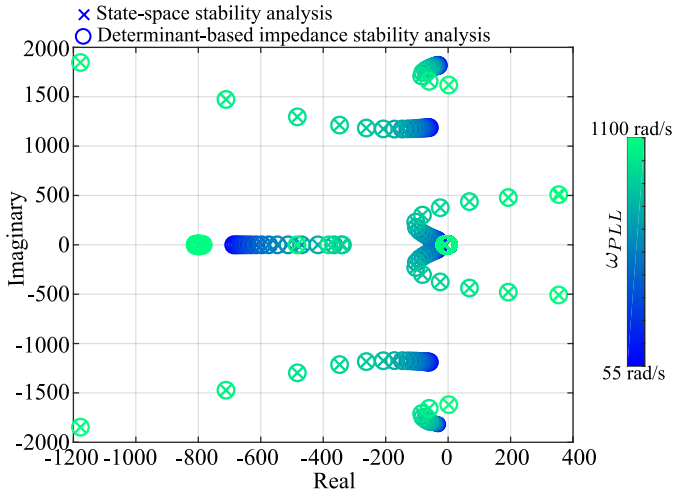

Figure 3. Pole locus: determinant-based impedance stability analysis vs. state-space stability analysis.

Table 1. Parameters of the grid-connected inverter.

Symbol	Parameter	Value
S	Power rating	1000 kVA
V_g	rms l-l AC grid voltage	320 kV
L_f	LC filter inductor	48.9 mH
R_f	LC filter resistor	0.512 Ω
C_f	LC filter capacitor	2.05 μF
L_t	AC transformer inductor	48.9 mH
R_t	AC transformer leakage resistor	1.024 Ω
SCR	short circuit ratio	2 $(L:R=10:1)$
i_{cd}^*	d-axis current reference	1 p.u.
i_{cq}^*	q-axis current reference	−0.2 p.u.
ω_c	current control cut-off frequency	275 rad/s
ω_{PLL}	phase-locked loop cut-off frequency	800 rad/s

ω_c & ω_{PLL} are calculated via their PI parameters based on [17,18].

4. Coupling Influence on the dq Impedance Stability Analysis

As mentioned in Section 2, the couplings of the impedance-ratio matrix in the eigenvalue-based impedance stability analysis are difficult to include. If the couplings are ignored, the dq impedance stability analysis will lose accuracy. To consider the couplings, the determinant-based dq impedance stability analysis is used. Three cases below are presented to show the influence of the couplings on the stability analysis.

1. Ignoring couplings causes the error of the stability analysis via the time-domain simulation;
2. The influence of the couplings on the pole locus;
3. The error quantification for the coupling influence on the stability analysis.

The inverter system as shown in Figure 2 is used for the stability analysis, and its parameters are shown in Table 1. Time-domain simulation of the grid-connected current-controlled inverter system was built in MATLAB/Simulink. The pole map was used to show the stability analysis results.

4.1. Time-Domain Validation

Based on the determinant-based dq impedance stability analysis, the analysis results with considering couplings or without considering couplings are shown as the pole map in Figure 4a under the 301-rad/s cut-off frequency of the PLL. The right-plane poles appear when the couplings are considered. On the contrary, if the couplings were ignored, the analysis shows that the system was stable because all its poles still stayed in the left plane. The stability analysis results of both impedance stability analyses were mismatched.

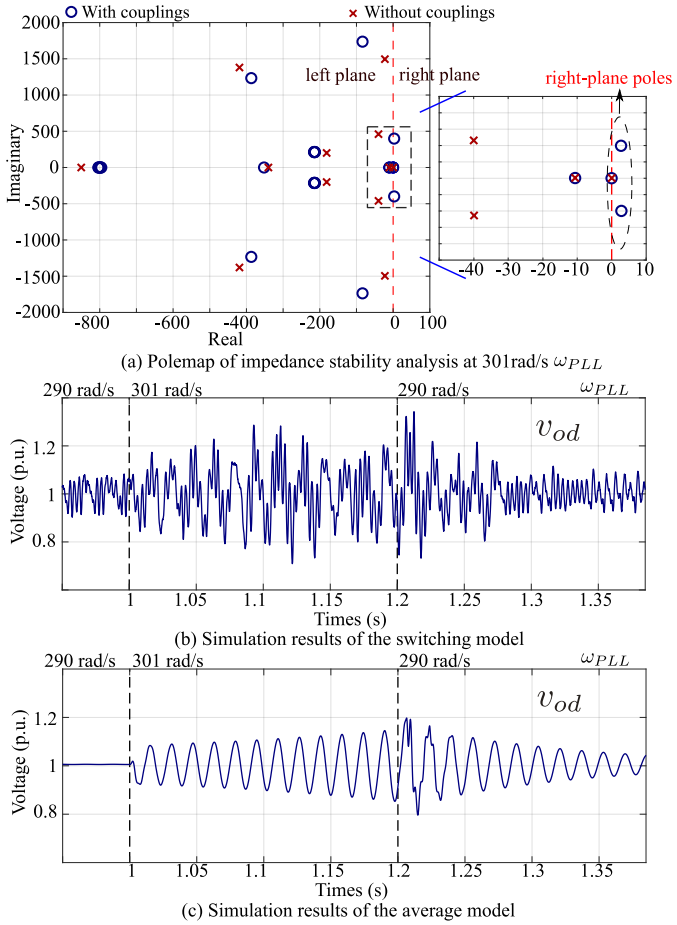

Figure 4. Time-domain simulation to validate the impedance stability analysis subject to $\omega_{PLL} = 290$ rad/s ($K^P_{PLL} = 410$ $K^i_{PLL} = 84{,}291$) and $\omega_{PLL} = 301$ rad/s ($K^P_{PLL} = 426$ $K^i_{PLL} = 90{,}863$).

The time-domain simulation of the grid-connected current-controlled inverter system was built in MATLAB/Simulink to validate the results from the stability analysis. The d-axis output voltage v_{od} was used to show the system state. The average model of the two-level VSCs was also added to show clearly that the system was unstable or became stable gradually without the disturbances of the harmonics.

As shown in Figure 4b,c, when the ω_{PLL} was increased from 290 rad/s to 301 rad/s at 1 s, v_{od} started to oscillate, and its magnitude increased gradually. It shows that the system was unstable at a 301-rad/s PLL cut-off frequency. At 1.2 s, the system was back to the stable condition as ω_{PLL} was changed back to 290 rad/s.

The time-domain simulation result at 301 rad/s ω_{PLL} matched the analysis result with the couplings, as shown in Figure 4a. Ignoring couplings failed to identify the instability. It proved that ignoring the couplings caused errors in the stability analysis.

4.2. Pole Locus Comparison

The coupling influence on the pole locus is drawn in this section. The influence of ignoring couplings on the pole locus is studied. Four pole locus are drawn via changing the parameters including ω_{PLL}, ω_c, i^*_{cd}, and i^*_{cq}, as shown in Figure 5.

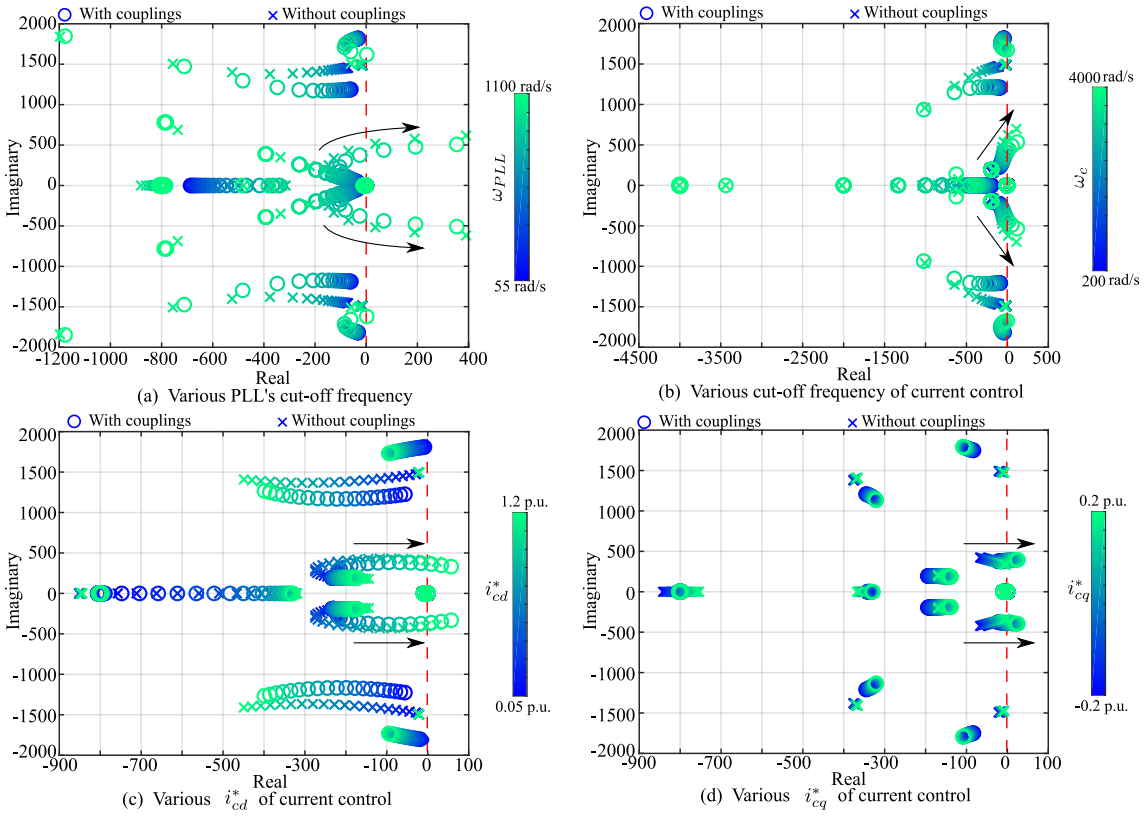

Figure 5. Pole locus: determinant-based impedance stability analysis vs. eigenvalue-based impedance stability analysis.

It is observed that the pole locus without considering the couplings was not precisely matched to the one with the couplings, as shown in Figure 5a–d. The movements of both pole loci were the same, but there were errors between each pair of poles.

For the movement, each pair of pole loci with or without coupling are shown in Figure 5a–d. The poles in the middle moved to the right-half plane when the parameters were increased significantly. Therefore, both impedance stability analyses can show that increasing ω_{PLL} (ω_c, i^*_{cd} and i^*_{cq}) reduced the system stability or even led to instability.

For the pole errors, it is observed that the error between each pair of poles always existed under the different values of the parameters, as shown in Figure 5a–d. These errors led the analysis without couplings to lose accuracy for the stability analysis. Furthermore, ignoring couplings could fail to identify the instabilities, as shown in Section 4.1.

4.3. Error Quantification for the Stability Analysis without Couplings

In this section, the error of the analysis without couplings is defined and shown. The cut-off frequency of the PLL, which is the basic control for the dq frame, was selected to determine the error, as shown below:

$$\text{error} = \frac{\omega_{PLL}^{E-max} - \omega_{PLL}^{D-max}}{\omega_{PLL}^{D-max}} \tag{35}$$

where ω_{PLL}^{E-max} are the maximum PLL cut-off frequency to keep the system stable based on the analysis without couplings. ω_{PLL}^{D-max} are the maximum PLL cut-off frequencies to keep the system stable based on the analysis with couplings.

ω_{PLL}^{E-max} and ω_{PLL}^{D-max} were identified by increasing ω_{PLL}^{E} and ω_{PLL}^{D} until their right-plane poles appeared in the pole map, respectively. Various SCRs were also selected to show the errors. The stability analysis errors based on (35) are therefore calculated and summarized in Table 2.

Table 2. Errors of the eigenvalue-based impedance stability analysis in terms of various SCRs.

Situation	ω_{PLL}^{D-max}	ω_{PLL}^{E-max}	Error
SCR = 2	298 rad/s	336 rad/s	12.7%
SCR = 5	802 rad/s	855 rad/s	6.6%
SCR = 10	1487 rad/s	1524 rad/s	2.5%
SCR = 15	1928 rad/s	1932 rad/s	0.2%

The error from the eigenvalue-based impedance stability analysis was 12.7% when the inverter connected to a weak AC grid (SCR = 2). It was reduced when the grid became stronger (SRC = 15); the error was only 0.2%. This is because the weak AC grid enhanced the couplings, and therefore, caused the large error in the eigenvalue-based impedance stability analysis.

The output voltage v_o (magnitude) was changed in terms of the various SCRs. The same operation point, that v_o at 1 p.u., should be maintained. i_{cq}^* was changed to achieve this in terms of various SCRs. The errors under the same magnitude of v_o are shown in Table 3.

Table 3. Errors of the eigenvalue-based impedance stability analysis in terms of various SCRs.

Situation	ω_{PLL}^{D-max}	ω_{PLL}^{E-max}	Error
SCR = 2, $i_{cq}^* = -0.2$	298 rad/s	336 rad/s	12.7%
SCR = 5, $i_{cq}^* = -0.05$	745 rad/s	817 rad/s	9.66%
SCR = 10, $i_{cq}^* = 0$	1332 rad/s	1471 rad/s	10.4%
SCR = 15, $i_{cq}^* = 0.04$	1682 rad/s	1876 rad/s	11.53%

It is observed that even a strong grid was connected, and the error (11.53%) was almost same as that of a week grid under the same output voltage operation point. No matter which type of AC grid was connected, the error from the eigenvalue-based impedance stability analysis could be around 10%, as shown in Table 3.

It was also found that ω_{PLL}^{D-max} increased along with the increasing SCR, as shown in Tables 2 and 3. When the inverter connects to a weak AC grid, ω_{PLL} should be reduced within the limit of ω_{PLL}^{D-max} in order to maintain the stable operation of the inverter system.

5. Conclusions

The coupling influence on the dq impedance stability analysis was studied. The results showed that ignoring the couplings of the impedance-ratio matrix brought significant errors up to 12.7% in the stability analysis, which may fail to identify the instabilities. The failure was validated in the time-domain simulation. Ignoring the couplings caused the wrong stability analysis results. A weak AC grid strengthened the couplings and caused the large errors. However, when the same output voltage magnitude of the inverter was maintained, the errors were around 10%, no matter whether a strong or a weak AC grid was connected. The couplings did not change the movement of the pole

locus. In other words, the analysis without couplings could still identify whether the stability was increased or decreased because of the changing parameters. The dq impedance stability analysis based on the determinant of the impedance-ratio matrix can achieve accurate stability analysis simply, which had the same accuracy as the state-space stability analysis.

For the future work, an auxiliary control will be designed based on the dq impedance stability analysis in order to stabilize the grid-connected inverter. The coupling influence on the outer loop control that regulates the power can be further studied via the impedance stability analysis.

Author Contributions: Author Contributions: Writing-Original Draft Preparation, C.L.; Writing-Review & Editing, T.Q., F.C., J.L., W.M., F.G. Supervision, X.G.

Funding: This research was funded by MIGRATE project under European Union's Horizon 2020 research and innovation program, grant number 691800.

Conflicts of Interest: The authors declare no conflict of interest.

Appendix A

The space matrix of the grid-connected inverter system is derived in this section for the state-space stability analysis. The state equation can be represented as:

$$s\widetilde{\mathbf{x}} = \mathbf{A}\widetilde{\mathbf{x}} + \mathbf{B}\widetilde{\mathbf{u}} \tag{A1}$$

where $\widetilde{\mathbf{x}}$ is the state vector, $\widetilde{\mathbf{u}}$ is the input vector, $\mathbf{A}$ is the state matrix, and $\mathbf{B}$ is the input matrix.

According to (A5), (A6), (A8), (A10), (A11), and (A16), $\widetilde{\mathbf{x}}$ is $[\widetilde{\theta}, \widetilde{x}_{PLL}, \widetilde{i}_{gd}, \widetilde{i}_{gq}, \widetilde{v}_{od}, \widetilde{v}_{oq}, \widetilde{x}_{cd}, \widetilde{x}_{cq}, \widetilde{i}_{cd}, \widetilde{i}_{cq}]^T$, and $\mathbf{A}$ is summarized into (A2). The eigenvalues of $\mathbf{A}$ are the poles that determine the system stability [2]. The details of the derivation are shown below.

$$\begin{bmatrix}
-K_{PLL}^p V_{od} & K_{PLL}^i & 0 & 0 & 0 & K_{PLL}^p & 0 & 0 & 0 & 0 \\
-V_{od} & 0 & 0 & 0 & 0 & 1 & 0 & 0 & 0 & 0 \\
0 & 0 & -\frac{R_g}{L_g} & \omega & \frac{1}{L_g} & 0 & 0 & 0 & 0 & 0 \\
0 & 0 & -\omega & -\frac{R_g}{L_g} & 0 & \frac{1}{L_g} & 0 & 0 & 0 & 0 \\
0 & 0 & -\frac{1}{C_f} & 0 & 0 & \omega & 0 & 0 & \frac{1}{C_f} & 0 \\
0 & 0 & 0 & -\frac{1}{C_f} & -\omega & 0 & 0 & 0 & 0 & \frac{1}{C_f} \\
-I_{cq} & 0 & 0 & 0 & 0 & 0 & 0 & 0 & -1 & 0 \\
I_{cd} & 0 & 0 & 0 & 0 & 0 & 0 & 0 & 0 & -1 \\
\frac{G_\theta^d}{L_f} & 0 & 0 & 0 & 0 & 0 & \frac{K_i^i}{L_f} & 0 & \frac{-K_i^p - R_f}{L_f} & 0 \\
\frac{G_\theta^q}{L_f} & 0 & 0 & 0 & 0 & 0 & 0 & \frac{K_i^i}{L_f} & 0 & \frac{-K_i^p - R_f}{L_f}
\end{bmatrix} \tag{A2}$$

The following relations are assumed:

$$\widetilde{v}_{oq}^s = s\widetilde{x}_{PLL} \tag{A3}$$

$$\begin{bmatrix} \widetilde{i}_{cd}^* \\ \widetilde{i}_{cq}^* \end{bmatrix} - \begin{bmatrix} \widetilde{i}_{cd}^s \\ \widetilde{i}_{cq}^s \end{bmatrix} = \begin{bmatrix} s\widetilde{x}_{cd} \\ s\widetilde{x}_{cq} \end{bmatrix} \tag{A4}$$

Substituting $\widetilde{v}^s_{oq}$ of (A3) with (19) yields:

$$s\widetilde{x}_{PLL} = -V_{od}\widetilde{\theta} + \widetilde{v}_{oq} \tag{A5}$$

Substituting $\widetilde{i}^s_{od}$ and $\widetilde{i}^s_{oq}$ of (A4) with (20) yields:

$$\begin{bmatrix} s\widetilde{x}_{cd} \\ s\widetilde{x}_{cq} \end{bmatrix} = \begin{bmatrix} -I_{cq}\widetilde{\theta} \\ I_{cd}\widetilde{\theta} \end{bmatrix} + \begin{bmatrix} -\widetilde{i}_{cd} \\ -\widetilde{i}_{cq} \end{bmatrix} + \begin{bmatrix} \widetilde{i}^*_{cd} \\ \widetilde{i}^*_{cq} \end{bmatrix} \tag{A6}$$

The relation of the phase-locked loop in Figure 2 can be summarized as:

$$s\widetilde{\theta} = \widetilde{v}^s_{oq}\frac{K^i_{PLL}}{s} + \widetilde{v}^s_{oq}K^p_{PLL} \tag{A7}$$

Substituting first $\widetilde{v}^s_{oq}$ with (A3) and second $\widetilde{v}^s_{oq}$ with (19) yields:

$$s\widetilde{\theta} = -K^p_{PLL}V_{od}\widetilde{\theta} + K^i_{pLL}\widetilde{x}_{PLL} + K^p_{PLL}\widetilde{v}_{oq} \tag{A8}$$

The relation between the voltage and the current induced by Z_g can be summarized below via the dq form:

$$\begin{bmatrix} \widetilde{v}_{od} \\ \widetilde{v}_{oq} \end{bmatrix} - \begin{bmatrix} \widetilde{v}_{gd} \\ \widetilde{v}_{gq} \end{bmatrix} = \begin{bmatrix} L_g s + R_g & -\omega L_g \\ \omega L_g & L_g s + R_g \end{bmatrix} \begin{bmatrix} \widetilde{i}_{gd} \\ \widetilde{i}_{gq} \end{bmatrix} \tag{A9}$$

Rearranging the equation yields:

$$\begin{bmatrix} s\widetilde{i}_{gd} \\ s\widetilde{i}_{gq} \end{bmatrix} = \begin{bmatrix} -\frac{R_g}{L_g} & \omega \\ -\omega & -\frac{R_g}{L_g} \end{bmatrix} \begin{bmatrix} \widetilde{i}_{gd} \\ \widetilde{i}_{gq} \end{bmatrix} + \begin{bmatrix} \frac{1}{L_g}\widetilde{v}_{od} \\ \frac{1}{L_g}\widetilde{v}_{oq} \end{bmatrix} + \begin{bmatrix} -\frac{1}{L_g}\widetilde{v}_{gd} \\ -\frac{1}{L_g}\widetilde{v}_{gq} \end{bmatrix} \tag{A10}$$

Following the same way, the relation over C_f can be arranged as:

$$\begin{bmatrix} s\widetilde{v}_{od} \\ s\widetilde{v}_{oq} \end{bmatrix} = \begin{bmatrix} -\frac{1}{C_f}\widetilde{i}_{gd} \\ -\frac{1}{C_f}\widetilde{i}_{gq} \end{bmatrix} + \begin{bmatrix} 0 & \omega \\ -\omega & 0 \end{bmatrix} \begin{bmatrix} \widetilde{v}_{od} \\ \widetilde{v}_{oq} \end{bmatrix} + \begin{bmatrix} \frac{1}{C_f}\widetilde{i}_{cd} \\ \frac{1}{C_f}\widetilde{i}_{cq} \end{bmatrix} \tag{A11}$$

The relation over Z_f can be found:

$$\begin{bmatrix} s\widetilde{i}_{cd} \\ s\widetilde{i}_{cq} \end{bmatrix} = \begin{bmatrix} -\frac{R_f}{L_f} & \omega \\ -\omega & -\frac{R_f}{L_f} \end{bmatrix} \begin{bmatrix} \widetilde{i}_{cd} \\ \widetilde{i}_{cq} \end{bmatrix} + \begin{bmatrix} \frac{1}{L_f}\widetilde{v}_{cd} \\ \frac{1}{L_f}\widetilde{v}_{cq} \end{bmatrix} + \begin{bmatrix} -\frac{1}{L_f}\widetilde{v}_{od} \\ -\frac{1}{L_f}\widetilde{v}_{oq} \end{bmatrix} \tag{A12}$$

$\widetilde{\mathbf{v}}_c$ is derived from the current control:

$$\begin{bmatrix} \widetilde{v}^s_{cd} \\ \widetilde{v}^s_{cq} \end{bmatrix} = \frac{K^i_i}{s}\left(\begin{bmatrix} \widetilde{i}^*_{cd} \\ \widetilde{i}^*_{cq} \end{bmatrix} - \begin{bmatrix} \widetilde{i}^s_{cd} \\ \widetilde{i}^s_{cq} \end{bmatrix} \right) + K^p_i\left(\begin{bmatrix} \widetilde{i}^*_{cd} \\ \widetilde{i}^*_{cq} \end{bmatrix} - \begin{bmatrix} \widetilde{i}^s_{cd} \\ \widetilde{i}^s_{cq} \end{bmatrix} \right) + \begin{bmatrix} 0 & -\omega L_f \\ \omega L_f & 0 \end{bmatrix} \begin{bmatrix} \widetilde{i}^s_{cd} \\ \widetilde{i}^s_{cq} \end{bmatrix} + \begin{bmatrix} \widetilde{v}^s_{od} \\ \widetilde{v}^s_{oq} \end{bmatrix} \tag{A13}$$

Replacing the first $\begin{bmatrix} \widetilde{i}^{*}_{cd} \\ \widetilde{i}^{*}_{cq} \end{bmatrix} - \begin{bmatrix} \widetilde{i}^{s}_{cd} \\ \widetilde{i}^{s}_{cq} \end{bmatrix}$ in (A13) with (A4) yields:

$$\begin{bmatrix} \widetilde{v}^{s}_{cd} \\ \widetilde{v}^{s}_{cq} \end{bmatrix} = K^{i}_{i} \begin{bmatrix} \widetilde{x}_{cd} \\ \widetilde{x}_{cq} \end{bmatrix} + K^{p}_{i} \left(\begin{bmatrix} \widetilde{i}^{*}_{cd} \\ \widetilde{i}^{*}_{cq} \end{bmatrix} - \begin{bmatrix} \widetilde{i}^{s}_{cd} \\ \widetilde{i}^{s}_{cq} \end{bmatrix} \right) + \begin{bmatrix} 0 & -\omega L_f \\ \omega L_f & 0 \end{bmatrix} \begin{bmatrix} \widetilde{i}^{s}_{cd} \\ \widetilde{i}^{s}_{cq} \end{bmatrix} + \begin{bmatrix} \widetilde{v}^{s}_{od} \\ \widetilde{v}^{s}_{oq} \end{bmatrix} \tag{A14}$$

Substituting $\widetilde{\mathbf{v}}^{s}_{c}$ in (21) with (A14) and substituting $\widetilde{\mathbf{i}}_{c}$, $\widetilde{\mathbf{v}}_{o}$ in (A14) with (19), (20) yield:

$$\begin{bmatrix} \widetilde{v}_{cd} \\ \widetilde{v}_{cq} \end{bmatrix} = \begin{bmatrix} G^{d}_{\theta}\widetilde{\theta} \\ G^{q}_{\theta}\widetilde{\theta} \end{bmatrix} + \begin{bmatrix} K^{i}_{i}\widetilde{x}_{cd} \\ K^{p}_{i}\widetilde{x}_{cq} \end{bmatrix} + \begin{bmatrix} -K^{p}_{i} & -\omega L_f \\ \omega L_f & -K^{p}_{i} \end{bmatrix} \begin{bmatrix} \widetilde{i}_{cd} \\ \widetilde{i}_{cq} \end{bmatrix} + \begin{bmatrix} K^{p}_{i}\widetilde{i}^{*}_{cd} \\ K^{p}_{i}\widetilde{i}^{*}_{cq} \end{bmatrix} + \begin{bmatrix} \widetilde{v}_{od} \\ \widetilde{v}_{oq} \end{bmatrix} \tag{A15}$$

where $G^{d}_{\theta} = -K^{p}_{i} I^{q}_{c} + \omega L_f I^{d}_{c} + V^{q}_{o} - V^{q}_{c}$, $G^{q}_{\theta} = -K^{p}_{i} I^{d}_{c} + \omega L_f I^{q}_{c} - V^{d}_{o} + V^{d}_{c}$.

Substituting $\widetilde{\mathbf{v}}_{c}$ in (A12) yields:

$$\begin{bmatrix} s\widetilde{i}_{cd} \\ s\widetilde{i}_{cq} \end{bmatrix} = \begin{bmatrix} \frac{G^{d}_{\theta}}{L_f}\widetilde{\theta} \\ \frac{G^{q}_{\theta}}{L_f}\widetilde{\theta} \end{bmatrix} + \begin{bmatrix} \frac{K^{i}_{i}}{L_f}\widetilde{x}_{cd} \\ \frac{K^{p}_{i}}{L_f}\widetilde{x}_{cq} \end{bmatrix} + \begin{bmatrix} \frac{-K^{p}_{i} - R_f}{L_f}\widetilde{i}_{cd} \\ \frac{-K^{p}_{i} - R_f}{L_f}\widetilde{i}_{cq} \end{bmatrix} + \begin{bmatrix} K^{p}_{i}\widetilde{i}^{*}_{cd} \\ K^{p}_{i}\widetilde{i}^{*}_{cq} \end{bmatrix} \tag{A16}$$

References

1. Liserre, M.; Teodorescu, R.; Blaabjerg, F. Stability of photovoltaic and wind turbine grid-connected inverters for a large set of grid impedance values. *IEEE Trans. Power Electron.* **2006**, *21*, 263–272. [CrossRef]
2. Kundur, P. *Power System Stability and Control*; McGraw-Hill, Inc.: New York, NY, USA, 1994; Chapter 12, pp. 699–822.
3. Sun, J. Impedance-Based Stability Criterion for Grid-connected Inverters. *IEEE Trans. Power Electron.* **2011**, *26*, 3075–3078. [CrossRef]
4. Wen, B.; Boroyevich, D.; Burgos, R.; Mattavelli, P.; Shen, Z. Inverse Nyquist Stability Criterion for Grid-Tied Inverters. *IEEE Trans. Power Electron.* **2017**, *32*, 1548–1556. [CrossRef]
5. MacFarlane, A.; Postlethwaite, I. The generalized Nyquist stability criterion and multivariable root loci. *Int. J. Control* **1977**, *25*, 81–127. [CrossRef]
6. Wen, B.; Boroyevich, D.; Mattavelli, P.; Shen, Z.; Burgos, R. Influence of Phase-locked loop on input damittance of three-phase voltage-source converters. In Proceedings of the 2013 Twenty-Eighth Annual IEEE Applied Power Electronics Converence and Exposition(APEC), Long Beach, CA, USA, 17–21 March 2013; pp. 897–904.
7. Harnefors, L.; Bongiorno, M.; Lundberg, S. Input-Admittance Calculations and Shaping for Controlled Voltage-Source Converters. *IEEE Trans. Ind. Electron.* **2007**, *54*, 3323–3334. [CrossRef]
8. Wen, B.; dushan Boroyevich.; Burgos, R.; Mattavelli, P.; Shen, Z. Analysis of D-Q Small-Signal Impedance of Grid-Tied Inverters. *IEEE Trans. Power Electron.* **2016**, *31*, 675–687. [CrossRef]
9. Burgos, R.; Boroyevich, D.; Wang, F.; Karimi, K.; Francis, G. On the Ac stability of high power factor three-phase rectifiers. In Proceedings of the 2010 IEEE Energy Conversion Congress and Exposition, Atlanta, GA, USA, 12–16 September 2010; pp. 2047–2054.
10. Cespedes, M.; Sun, J. Impedance Modeling and Analysis of Grid-Connected Voltage-Source Converters. *IEEE Trans. Power Electron.* **2014**, *29*, 1254–1261. [CrossRef]
11. kazem Bakhshizadeh, M.; Wang, X.; Blaabjerg, F.; Hjerrild, J.; Kocewiak, L.; Bak, C.L.; Hesslbak, B. Couplings in Phase Domain Impedance Modeling of Grid-Connected Converters. *IEEE Trans. Power Electron.* **2016**, *31*, 6792–6797.
12. Hiti, S.; Vlatkovic, V.; Borojevic, D.; Lee, F.C. A new control algorithm for three-phase PWM buck rectifier with input displacement factor compensation. In Proceedings of the IEEE Power Electronics Specialist Conference (PESC'93), Seatle, WA, USA, 20–24 June 1993; pp. 648–654.
13. Mao, H.; Boroyevich, D.; Lee, F.C.Y. Novel reduced-order small-signal model of a three-phase PWM rectifier and its application in control design and system analysis. *IEEE Trans. Power Electron.* **1998**, *13*, 511–521.

14. Cao, W.; Ma, Y.; Yang, L.; Wang, F.; Tolbert, L.M. D-Q Impedance Based Stability Analysis and Parameter Design of Three-Phase Inverter-Based AC Power Systems. *IEEE Trans. Ind. Electron.* **2017**, *64*, 6017–6028. [CrossRef]
15. Xu, Y.; Nian, H.; Wang, T.; Chen, L.; Zheng, T. Frequency Coupling Characteristic Modeling and Stability Analysis of Doubly Fed Induction Generator. *IEEE Trans. Energy Convers.* **2018**, *33*, 1475–1486. [CrossRef]
16. Zhang, C.; Cai, X.; Rygg, A.; Molinas, M. Sequence domain siso equivalent models of a grid-tied voltage source converter system for small-signal stability analysis. *IEEE Trans. Energy Convers.* **2018**, *33*, 741–749. [CrossRef]
17. Chung, S.K. A Phase Tracking System for Three Phase Utility Interface Inverters. *IEEE Trans. Power Electron.* **2000**, *15*, 431–438. [CrossRef]
18. Yazdani, A.; Iravani, R.*Voltage-Sourced Converters in Power Systems*; John Wiley & Sons, Inc.: Hoboken, NJ, USA; 2010; Chapter 8, pp. 204–205.